Journal of Materials Chemistry C

Synergistic effect of carotenoid and silicone-based additives for photooxidatively stable organic solar cells with enhanced elasticity

Journal:	*Journal of Materials Chemistry C*
Manuscript ID	TC-ART-04-2021-001544.R1
Article Type:	Paper
Date Submitted by the Author:	07-Jun-2021
Complete List of Authors:	Prete, Michela; University of Southern Denmark, Mads Clausen Institute Ogliani, Elisa; Technical University of Denmark, Chemical and Biochemical Engineering Bregnhøj, Mikkel; Aarhus University, Chemistry Sandby Lissau, Jonas; University of Southern Denmark, Mads Clausen Institute Dastidar, Subham; The University of Arizona College of Engineering, Chemical and Environmental Engineering Rubahn, Horst-Gunter; University of Southern Denmark, Mads Clausen Institute, NanoSYD Engmann, Sebastian; NIST, ; Theiss Research, Skov, Anne; Technical University of Denmark, Chemical and Biochemical Engineering Brook, Michael; McMaster University Department of Chemistry & Chemical Biology, Chemistry and Chemical Biology Ogilby, Peter; Aarhus University, Chemistry Printz, Adam; The University of Arizona College of Engineering, Chemical & Environmental Engineering Turkovic, Vida; University of Southern Denmark Madsen, Morten; NanoSYD, University of Southern Denmark, University of Southern Denmark, MCI, SDU NanoSYD

ARTICLE

Synergistic effect of carotenoid and silicone-based additives for photooxidatively stable organic solar cells with enhanced elasticity

Received 00th January 20xx,
Accepted 00th January 20xx

DOI: 10.1039/x0xx00000x

Michela Prete[a], Elisa Ogliani[b], Mikkel Bregnhøj[c], Jonas Sandby Lissau[a], Subham Dastidar[d], Horst-Günter Rubahn[a], Sebastian Engmann[e,f], Anne Ladegaard Skov[b], Michael A. Brook[g], Peter R. Ogilby[c], Adam Printz[*d], Vida Turkovic[*a] and Morten Madsen[*a]

Photochemical and mechanical stability are critical in the production and application of organic solar cells. While these factors can individually be improved using different additives, there is no example of studies on the combined effects of such additive-assisted stabilization. In this study, the properties of PTB7:[70]PCBM organic solar cells are studied upon implementation of two additives: the carotenoid astaxanthin (AX) for photochemical stability and the silicone polydimethylsiloxane (PDMS) for improved mechanical properties. A newly designed additive, AXcPDMS, based on astaxanthin covalently bonded to PDMS was also examined. Lifetime tests, produced in ISOS-L-2 conditions, reveal an improvement in the accumulated power generation (APG) of 10 % with pure AX, of 90 % when AX is paired with PDMS, and of 140 % when AXcPDMS is added in the active layer blend, as compared to the control devices. Singlet oxygen phosphorescence measurements are utilized to study the ability of AX and AXcPDMS to quench singlet oxygen and its precursors in the films. The data are consistent with the strong stabilization effect of the carotenoids. While AX and AXcPDMS are both efficient photochemical stabilizers, the improvement in device stability observed in the presence of AXcPDMS is likely due to a more favorable localization of the stabilizer within the blend. The mechanical properties of the active layers were investigated by tensile testing and cohesive fracture measurements, showing a joint improvement of the photooxidative stability and the mechanical properties, thus yielding organic solar cell devices that are promising for flexible photovoltaic applications.

Introduction

The field of organic photovoltaics (OPV) is rapidly evolving, demonstrating a strong potential to contribute to the green energy transition towards a fully carbon-neutral economy and society (1,2). The recently achieved world record power conversion efficiency (3–5) (PCE) of 18.2 % for single junction (1) and 17.3 % for multijunction (2) OPV, along with low cost, light weight, flexibility, free form design, low environmental impact and short energy payback time, are just some indicators of the great potential of this technology. With the recent efficiency boost (6,7), the research priority is now to find solutions to keep that initially high efficiency over the time of use and extend the otherwise relatively short lifetime of the devices (8–13). OPV devices must withstand harsh fabrication and operational conditions, making the topic of device stability an important focus of research efforts within the OPV field. When considering the stability of flexible organic solar cells, three main processes jointly affect device performance: morphological(14), photooxidative (15) and mechanical (16) degradation. Although the morphology of the active layer in the as-cast devices can be manipulated by various processing techniques to achieve high performance, the repulsive molecular interactions between the donor and acceptor molecules can over time lead to a spontaneous phase separation in the solid state (17–19). Progress with morphological stability has been achieved with certain types of non-fullerene acceptor molecules (9,20–23) which, due to their high glass transition temperatures (24,25), planarity and bulkiness, have a lower diffusion coefficient which also reduces the rate of crystallization and phase separation and thus provides a higher donor/acceptor blend stability than the fullerene acceptor molecules (26).

Photochemical stability invariably involves adverse effects of molecular oxygen, particularly when the device is illuminated. One approach for stabilization is thus encapsulation with barrier and getter materials (27–32). However, many barriers, like

[a] SDU NanoSYD, Mads Clausen Institute, University of Southern Denmark, Alsion 2, 6400 Sønderborg, Denmark
[b] Department of Chemical and Biochemical Engineering, Technical University of Denmark, Søltofts Plads, 2800, Kgs. Lyngby, Denmark
[c] Department of Chemistry, Aarhus University, Langelandsgade 140, 8000 Aarhus, Denmark
[d] Department of Chemical and Environmental Engineering, The University of Arizona, 1133 E. James E. Rogers, Tucson, Arizona, 85721, United States
[e] Nanoscale Device Characterization Division, National Institute of Standards and Technology, 100 Bureau Drive, Gaithersburg, Maryland, 20899, United States
[f] Theiss Research, La Jolla, California, 92037, United States
[g] Department of Chemistry and Chemical Biology, McMaster University, 1280 Main St. W., Hamilton, Ontario L8S 4M1, Canada
Electronic Supplementary Information (ESI) available: [details of any supplementary information available should be included here]. See DOI: 10.1039/x0xx00000x

multi-layered oxides (e.g., Al_2O_3/SiO_2) or thick glass slides, can be incompatible with maintaining device flexibility and can also increase the fabrication costs. Some active layer instabilities can also be mitigated using certain interlayers, which either act as barriers or simply provides more stable interfaces towards the active layer (33–37). For the active layer itself, development of new molecules with inherently higher photooxidative stability is of great importance. However, most studies still focus primarily on achieving high initial power conversion efficiencies, regardless of the long-term stability of the devices (8,38–41). We follow an alternative approach; additive-assisted stabilization. In this method, a third component is blended into the OPV active layer, which can add functionality, such as interfering with radical chain oxidation processes, quenching the reactive oxygen species, or acting as a barrier to UV irradiation (42–55).

We have reported effective stabilization of OPV devices using several types of antioxidants: UV absorbers (45), hydroperoxide decomposers (42), hydrogen donors (43), and quenchers of singlet oxygen and its photosensitizing precursors (44,47). Similar approaches have also been reported in the literature (48–53,55). Recently, we reported an increase in device stability using the naturally occurring carotenoid β-carotene (44,47), where the stabilization effect arises from quenching of singlet oxygen and its sensitizer (in this case [70]PCBM triplet states), all together underlining the strong potency of naturally occurring antioxidants on improving the photochemical stability of high-performing OPV devices.

The mechanical properties of the active layer and OPV devices made thereof arise from the constituent donor and acceptor molecules and the morphology they adopt in blends (56–63). The molecular structure, such as the length of the alkyl solubilizing groups of donor molecules (56,58) or slight modifications in the polymer backbone (60), can greatly influence the elastic modulus. *Lipomi et al.* (16) demonstrated that in active layers of stretchable devices a higher elastic modulus correlates with an increased fragility, as determined by crack-onset measurements under the same stressing conditions. It has also been shown that the addition of insulating macromolecular additives (e.g., atactic polystyrene, poly(methyl methacrylate), high-density polyethylene) to the organic semiconductor blends, a concept introduced by numerous works of the *Stingelin* group (64–67), can enhance the mechanical robustness of resulting structures and add a protective encapsulation effect. The utilization of a macromolecular plasticizer in the active layer has also been reported by *Graham et al.* (68), and later extended by *Savagatrup et al.* (56), where low molecular weight polydimethylsiloxane (PDMS) was used to modify the active layer film morphology, lowering its elastic modulus and increasing the device PCE.

While there have been numerous studies on the use of antioxidants for improving the photooxidative stability and, independently, of plasticizers to enhance the morphological and mechanical properties of OPV active layers and devices, the effect of combining these approaches has not yet been reported. Besides, the possible influence of photooxidative stabilizers on the mechanical properties of OPV active layers has, again to our knowledge, not been assessed. In this study, we investigate the synergistic effect of antioxidants and plasticizers on the photooxidative stability and mechanical properties of OPV active layers. We report on the photooxidative stabilization of organic solar cells using the naturally occurring antioxidant astaxanthin, already shown to be an excellent quencher of both singlet oxygen ($O_2(a^1\Delta_g)$) and singlet oxygen photosensitizing precursors (44), and compare its stabilizing effect to that of astaxanthin covalently bonded to PDMS, a new molecule synthesized for this study. The intrinsic photooxidative stability, and improvement thereof, is assessed using ISOS-L-2 (1 Sun irradiation at 65°C in ambient air) (69) OPV device lifetime studies as well as singlet oxygen phosphorescence measurements, and the synergistic improvement of the mechanical properties is discussed in terms of the elastic modulus and cohesive fracture energies.

Results and discussion

Device Performance

OPV devices employing active layers based on the molecules shown in Figure 1 were developed and tested in this study. A commonly applied OPV blend was studied, consisting of the electron donor PTB7 matched to the electron acceptor [70]PCBM. It was previously shown that the main intermediate in the photooxidation of this system is singlet oxygen (44,47,48,70,71), thus efficient quenchers of singlet oxygen and the triplet states of its photosensitizing precursor molecules are required to stabilize it. Following up on our recent study on carotenoid antioxidants for photooxidative stabilization of OPV (44), we used astaxanthin (AX) as an antioxidant, PDMS as a plasticizer, and we synthesized a new covalent combination of the two additives, AXcPDMS, to investigate the effects of these additives on the OPV photooxidative stability and mechanical properties. The motivation for employing astaxanthin here, instead of β-carotene as previously reported (44,47), was the possibility to synthesize the new AXcPDMS compound as a

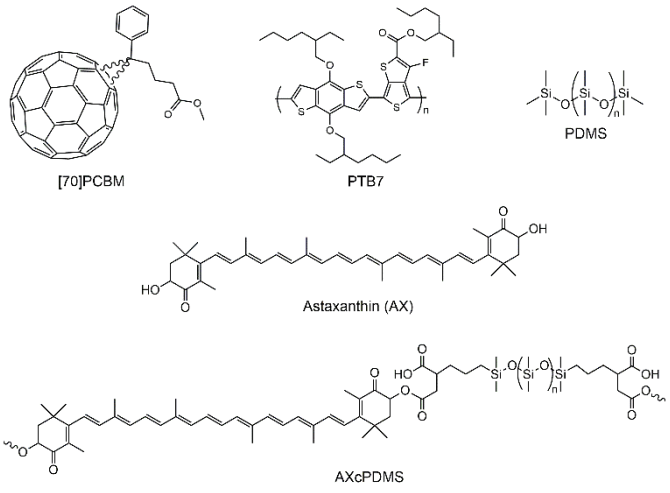

Figure 1 Molecular structures of the components used in the studied OPV active layer films and devices.

bifunctional antioxidant, which simultaneously provides photooxidative stability and enhances the mechanical properties of the OPV active layer. The hydroxyl groups at the ends of the AX molecule offer attachment points for the PDMS without affecting the conjugated double bonds and, presumably, the antioxidant properties of the additive.

The devices in this study were fabricated in the inverted configuration shown in Figure 2A, employing PTB7:[70]PCBM as active layers in between solution processed ZnO_x electron transport layers and thermally evaporated MoO_x hole transport layers. Representative J(V) curves are shown in Figure 2B with the photovoltaic parameters listed in Table 1. The concentration of additives was varied, keeping in mind that a higher concentration of additive will have a stronger positive effect on the device stability, but also possibly reduce the device performance. Thus, the additive concentration was increased only to the point at which devices retained at least 2/3 of the power conversion efficiency of pristine control devices.

The addition of 3 % by mass (wt%) of AX into PTB7:[70]PCBM devices resulted in an efficiency drop from 6.6 % to 4.5 %, mainly driven by the decrease in J_{sc} and FF, similar to the effect observed by adding β-carotene into this system (47). The addition of PDMS decreased the J_{sc} further from 10.6 mA/cm^2 to 9.8 mA/cm^2, but along with an increase in FF from 60.0 % to 64.6 %, it kept the PCE at a comparable level. To test the stabilizing effects of the newly synthesized additive, a similar concentration optimization was performed with up to 3 wt% AXcPDMS in the blends. When 3 wt% AXcPDMS was added in PTB7:[70]PCBM devices, a decrease of ~20 % in both the FF and J_{sc} parameters were observed, thus showing PCE values outside the selection criteria. Upon adding 0.3 wt% and 0.03 wt% of our novel additive AXcPDMS, there were no significant changes in the photovoltaic parameters when compared with the control devices.

Device lifetimes

As highlighted in our previous work (44), one process that can adversely affect organic solar cells is the reaction of molecules in the device with singlet oxygen, $O_2(a^1\Delta_g)$. Many of the light-absorbing molecules commonly incorporated into a solar cell can photosensitize the production of $O_2(a^1\Delta_g)$ by transfer of the photoexcitation energy to ground state oxygen, $O_2(X^3\Sigma_g^-)$. [70]PCBM is an efficient sensitizer of $O_2(a^1\Delta_g)$, and thus one route to stabilize this OPV system is to incorporate an efficient $O_2(a^1\Delta_g)$ quencher into the device. We have shown that, in solution, astaxanthin does not form ground state complexes with these donor and acceptor compounds. , More importantly, it mitigates the effects of $O_2(a^1\Delta_g)$ by quenching both its precursor (i.e., the [70]PCBM triplet state) and $O_2(a^1\Delta_g)$ itself (44).

We tested the stability of unencapsulated devices upon 70 h of continuous illumination following the ISOS-L-2 accelerated degradation protocol, i.e., exposure to 1 Sun irradiation at 65°C in ambient air. Figure 3A and Figure 3B report the stabilizing effect of the different additives utilized in this study. The strong decay of the reference devices has previously been attributed to singlet oxygen driven photooxidation (47,48,70).

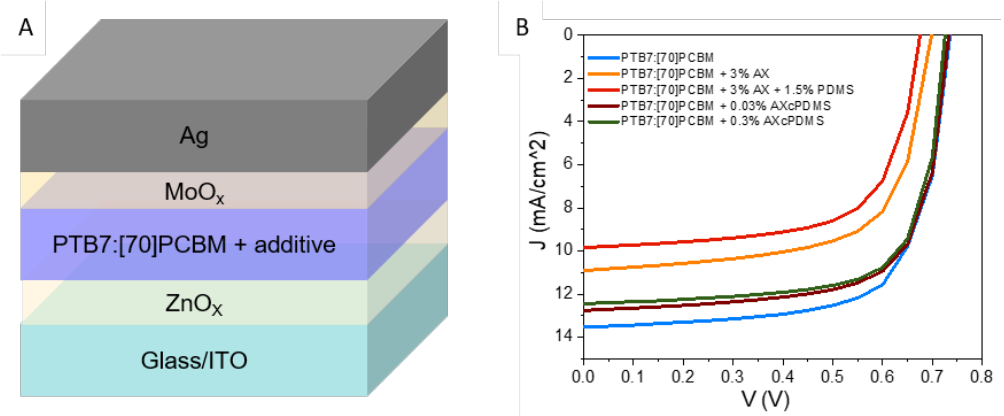

Figure 2 Structure (A) and J(V) characteristics (B) of PTB7:[70]PCBM organic photovoltaic cells with and without the additives investigated in this study

Table 1 Photovoltaic parameters of the OPV devices. Open circuit voltage (Voc), short-circuit current density (Jsc), fill factor (FF) and power conversion efficiency (PCE) of PTB7:[70]PCBM devices with and without the tested additives. Average values, along with and without the tested additives. Average values, along with the standard deviations, are extracted from at least 5 devices. Weight percentages of additives are calculated with respect to the total dry weight of donor and acceptor molecules in the active layer blend.

Device	V_{oc} [V]	J_{sc} [mA/cm^2]	FF [%]	PCE [%]
PTB7:[70]PCBM	0.72±0.01	13.1±0.4	69.7±4.6	6.6±0.5
PTB7:[70]PCBM + 3 wt% AX	0.70±0.04	10.6±0.7	60.0±5.0	4.5±0.6
PTB7:[70]PCBM + 1.5 wt% PDMS	0.73±0.01	13.0±0.2	67.1±5.0	6.3±0.4
PTB7:[70]PCBM + 3 wt% AX + 1.5 wt% PDMS	0.68±0.01	9.8±0.1	64.6±2.2	4.3±0.2
PTB7:[70]PCBM + 3 wt% AXcPDMS	0.72±0.04	10.8±0.4	48.5±2.9	3.8±0.2

PTB7:[70]PCBM + 0.3 wt% AXcPDMS	0.73±0.01	12.1±0.2	69.8±2.3	6.1±0.3
PTB7:[70]PCBM + 0.03 wt% AXcPDMS	0.70±0.03	12.5±0.5	69.1±3.5	6.1±0.5

As shown in Figure 3, upon addition of 3 wt% of AX (orange line) into the PTB7:[70]PCBM active layer blend, the stability of the devices was slightly enhanced as compared to the reference devices (cyan line). While the addition of a plasticizer is known to promote a higher degree of mobility of the polymer chains, increasing the disorder within the blend and more readily allowing permeation by oxygen (72–74), we observed here that adding 1.5 wt% PDMS together with AX in the active layer (red line) slightly increased the device stability. Interestingly, the strongest stabilization effect was achieved when AXcPDMS was inserted in the PTB7:[70]PCBM blend, both in 0.3 wt% (dark green line) and 0.03 wt% (dark red line). The data in Figure 3 can be quantified using a bi-exponential decay function and the extracted figures of merit (47) are listed in Table 2. The additive´s stabilization effect was also evident from the comparison of accumulated power generation (APG; which is and the bi-exponentially fitted device efficiency over their lifetime (47)) which was 10 % enhanced for AX alone, 90 % enhanced for AX and PDMS together, and 140 % increased for AXcPDMS, as compared to the reference devices without additives (Table 2). As AXcPDMS contains the same functional groups as AX and PDMS alone (Figure 1), linking these two components may influence the way in which this additive is distributed across the active layer. The prerequisite for effective photooxidative stabilization is the physical proximity of the added quencher to the singlet oxygen precursor or singlet oxygen itself (75). In PTB7:[70]PCBM systems, it has been shown that it is the [70]PCBM molecules that are the dominant singlet oxygen sensitizers in the blend (44,47). Thus, we can infer that AXcPDMS presumably localizes in a more favourable position to quench the [70]PCBM triplet excited states before singlet oxygen can be produced.

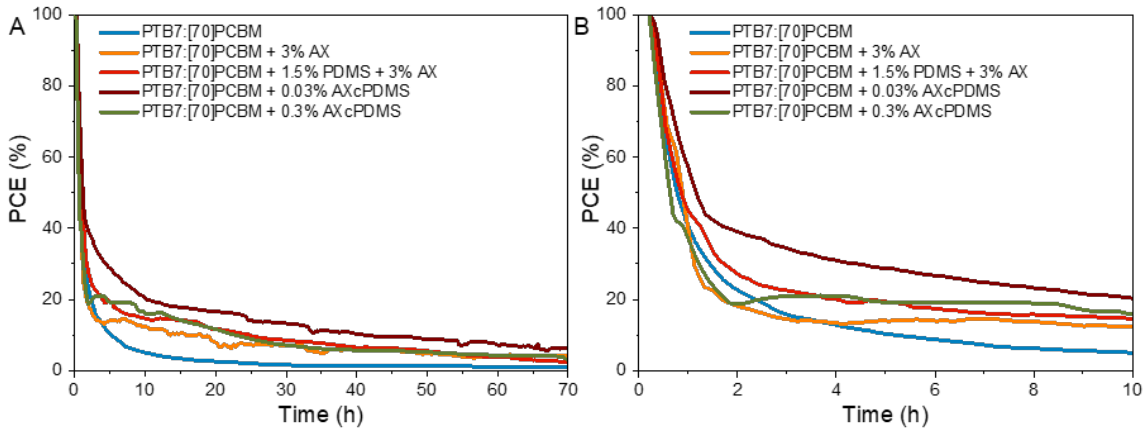

Figure 3 Lifetime measurements conducted according to ISOS-L-2 protocol standards, of PTB7:[70]PCBM devices with and without additives (a). Zoom of the first 10 h of degradation (b).

defined as the integrated product of the incident light power

Table 2 Common device lifetime performance parameters for PTB7:[70]PCBM devices compared with the devices containing different additives. Shown are the extracted initial power conversion efficiency (PCE_0), the accumulated power generated over the lifetime of the device ($APG_{lifetime}$), the burn-in time ($t_{burn-in}$), the efficiency at the end of the burn-in period ($PCE_{burn-in}$), time at which PCE is reduced to 80 % compared to the burn-in (t_{T80}), and the period between burn-in and T_{80} (i.e., the lifetime of the device, $t_{lifetime}$). Fitted parameters and standard errors are shown in Supplementary 1.

	PTB7:[70]PCBM	PTB7:[70]PCBM + 3 wt% AX	PTB7:[70]PCBM + 3 wt% AX + 1.5 wt% PDMS	PTB7:[70]PCBM + 0.3 wt% AXcPDMS	PTB7:[70]PCBM + 0.03 wt% AXcPDMS
PCE_0 [%]	6.6	4.5	4.3	6.1	6.1
$APG_{lifetime}$ [Wh/m²]	49.7	54.8	96.8	84.9	120.3
$t_{burn-in}$ [h]	2.7	4.0	4.4	3.8	3.9
$PCE_{burn-in}$ [%]	1.1	0.9	0.9	1.8	1.7
t_{T80} [h]	3.8	6.0	11.3	6.2	8.4
$t_{lifetime}$ [h]	1.1	2.0	6.9	2.5	4.5

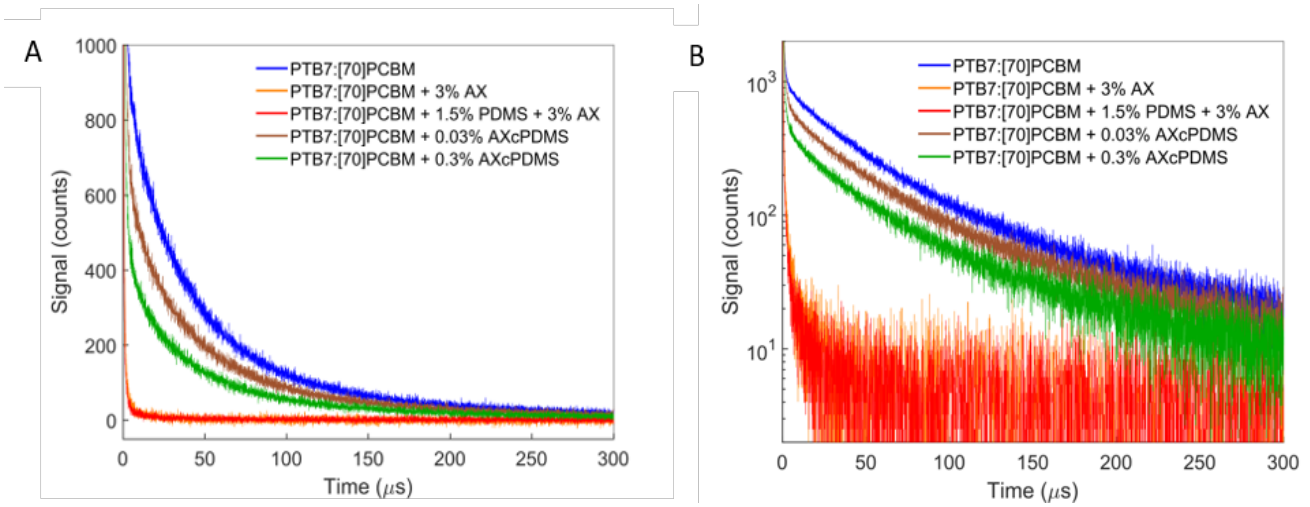

Figure 4 Time-resolved singlet oxygen phosphorescence signals recorded from PTB7:[70]PCBM films. A) Data recorded on films with different additives. B) The same dataset plotted in a semi-logarithmic scale. In both panels, the red trace covers the orange trace.

Singlet oxygen phosphorescence

The presence and decay kinetics of singlet oxygen in PTB7:[70]PCBM active layer films, with and without the additives, was directly probed using time-resolved singlet oxygen phosphorescence measurements, as shown in Figure 4 and Supplementary 2. Because the amount of singlet oxygen formed is dependent on the [70]PCBM concentration (47), the [70]PCBM to PTB7 ratio in the tested films was kept at 3:1 to allow for singlet oxygen detection with an acceptable signal-to-noise ratio. As is evident in Figure 4, PTB7:[70]PCBM films without additives yield a clear singlet oxygen signal. In the presence of 3 wt% AX, the singlet oxygen signal is appreciably quenched. From our previous study, we infer that AX efficiently quenches both the singlet oxygen precursor (the [70]PCBM triplet state) and singlet oxygen itself, reducing both the amplitude and lifetime of the signal (44,47).

The same observations apply for films with 3 wt% AX + 1.5 wt% PDMS. When only PDMS is added to the system, an appreciable singlet oxygen signal (data not shown here), comparable to that of the reference sample without additives, was measured demonstrating that, as expected, PDMS itself does not appreciably quench singlet oxygen (76). Upon addition of 0.03 wt% and 0.3 wt% of the covalently bonded AXcPDMS, the singlet oxygen signal is also suppressed as compared to the control sample. However, as is evident from the semi-logarithmic graph in Figure 4B, the main reduction occurs in the amplitude of the signal, whereas the lifetime remains virtually unchanged at these quencher concentrations. This indicates that the dominant quenching is of the singlet oxygen precursors, i.e., the PCBM triplet states, as opposed to that of the singlet oxygen itself.

Steady-state and transient photoluminescence

Photoluminescence (PL) and time-resolved photoluminescence (TRPL) were utilized to gather further information about the exciton decay processes taking place inside the active layer blends. We note that both donor and acceptor excited states are populated at the excitation wavelength of ~ 395 nm used in this study, although the absorbance of [70]PCBM is larger at this wavelength. Figure 5a shows the steady-state photoluminescence spectra of the active layers containing different additives, with a photoluminescence peak at around 740 nm. The PL emission is consistent with that of [70]PCBM excitons, as seen when comparing to the PL spectrum of a pure [70]PCBM film (see Supplementary 3 and 4). This spectrum is also consistent with fast energy transfer from PTB7 to [70]PCBM typically reported for this system (77). The PL peak at 740 nm is at slightly lower photon energies compared to a study by the *Dyakonov* group (78), but still easily distinguished from that of PTB7. The lifetime of the emission, shown in Figure 5b, is relatively short, consistent with an assignment to [70]PCBM singlet excitons (79). We note that while triplet-charge annihilation (80) could, in principle, reduce the lifetime of triplet excitons significantly in such blend systems, the lifetimes observed here are sufficiently short, and triplet state emission is generally sufficiently weak, that the observed signal does likely not include contributions from triplet exciton phosphorescence. The TRPL spectra can be fitted to bi-exponentially decaying functions showing a weighted average lifetime of 125 ps for the reference sample. Adding 3 % AX reduces the lifetime of the signal to 31 ps. This latter value is approaching the time resolution limit of the detection system but is still significantly shorter than the value recorded for the reference sample. As such, we infer that AX, when added in amounts of 3 %, significantly quenches the initially populated singlet excitons of [70]PCBM, or perturbs the morphology of the blend so that singlet excitons are faster separated into free charges at the donor and acceptor interface, thus lowering the singlet exciton lifetime. We note that the latter could take place due to smaller domain sizes of [70]PCBM upon addition of the AX additive, which is also supported by the interaction

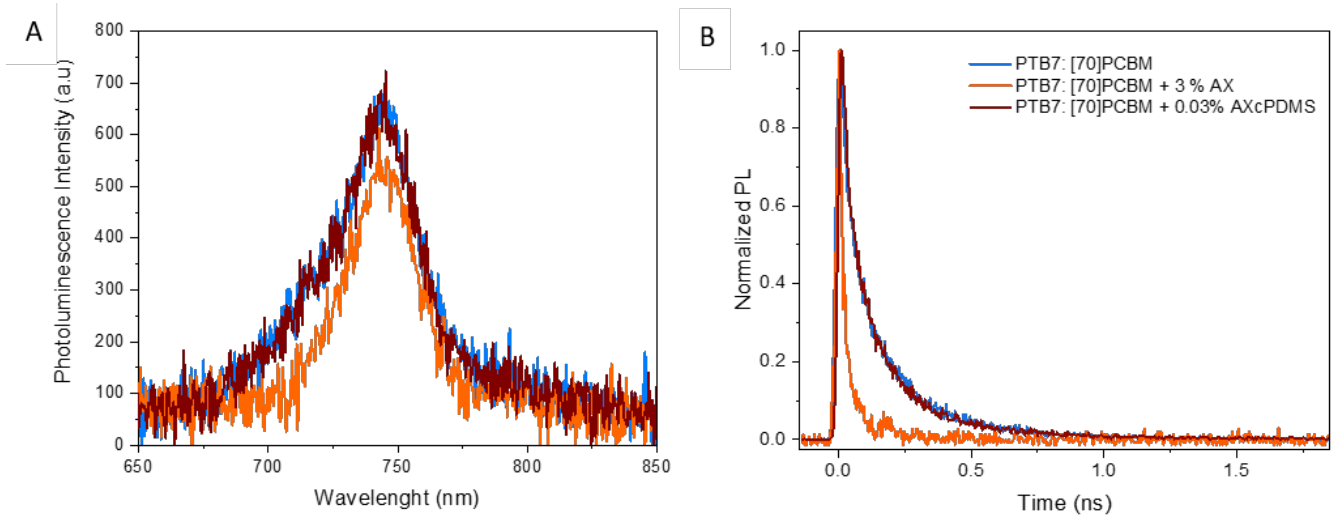

Figure 5 a) Steady-state photoluminescence (PL) spectrum of PTB7:[70]PCBM films with selected additive combinations. b) Time-resolved photoluminescence traces of the same samples recorded at the peak wavelength of 740 nm.

parameters of the blend constituents, with [70]PCBM preferably mixing with both PTB7 and AX (see Supplementary 5). These effects may lead to a reduction of the amounts of triplet excitons and singlet oxygen formed downstream (Figure 4), which is reflected in the longer lifetime of the device (Table 2). We note that the power conversion efficiency for fresh devices is lower upon addition of AX, due to the lower FF and Jsc, which could arise due to the above effects. The overall result is only a modest increase in the overall accumulated power generation over the lifetime of the device (Table 2).

In contrast, the addition of 0.03 % AXcPDMS does, within experimental uncertainty, not change the lifetime of the TRPL signal and the [70]PCBM singlet excitons, leaving the photovoltaic performance virtually unaffected. Considering that AXcPDMS is, unlike AX, a large polymeric additive consisting largely of PDMS (which has a very poor interaction with both of the active layer molecules), the unperturbed TRPL signal might be understood in terms of active layer morphology unperturbed by AXcPDMS. However, 0.03 % AXcPDMS is sufficient to partially quench the longer-lived triplet excitons, resulting in reduced singlet oxygen production and a significantly prolonged device lifetime, due to a shortened burn-in period. As reported previously, the main cause of burn-in in PTB7:[70]PCBM system is singlet oxygen (47). We note, that increasing the concentration of AXcPDMS to 0.3 % does indeed reduce the production of singlet oxygen even further (Figure 4), but also adversely affect the photovoltaic performance over time. As such, 0.03 % is closer to the optimal additive concentration for this system.

Elastic modulus and cohesive fracture energy

The elastic modulus (E_f) of the active layers containing different additives was determined from films spin coated on glass from chlorobenzene (CB) solutions (Figure 6A). The elastic modulus of the reference PTB7:[70]PCBM of 2.19 ± 0.37 GPa agrees with the previously reported values by Kim J. et al. (81) of 2.01 ± 0.14 GPa for 1:2 polymer to fullerene ratio. For PTB7:[70]PCBM + 3 wt% AX the elastic modulus was lowered to 1.27 ± 0.29 GPa, indicative of a highly improved film flexibility, giving such devices an advantage in reliability for flexible applications (82). The reason for this might be in the preferred interaction of AX with [70]PCBM, which as a consequence disturbs the formation of pure crystalline phases of PTB7, leading to less stiff films. Surprisingly, upon addition of 1.5 wt% of elastomeric additive PDMS, the tensile modulus of the films remained comparable to the reference, 1.98 ± 0.44 GPa. The similar modulus might be explained by the low miscibility of PDMS with PTB7 and [70]PCBM, as indicated by the corresponding interaction parameters (see Supplementary 5) preventing PDMS from blending uniformly within the active layer. This would be required to pass on its inherent compliance to the resulting active layer films. A similar E_f, 2.36 ± 0.22 GPa, was observed when 1.5 wt% of PDMS was blended together with 3 wt% AX into the active layers, where the positive effect of AX intercalating into [70]PCBM is somewhat obstructed by the interaction with PDMS.

Table 3 Cohesive fracture energies, G_c, of the different PTB7:[70]PCBM bulk heterojunctions with all the additives combinations.

Sample	Elastic Modulus [GPa]	Cohesive Fracture Energy [J/m^2]
PTB7:[70]PCBM	2.19±0.37	1.32±0.40
PTB7:[70]PCBM + 3 wt% AX	1.27±0.29	2.03±0.57
PTB7:[70]PCBM + 1.5 wt% PDMS	1.98±0.44	1.38±0.52
PTB7:[70]PCBM + 3 wt% AX + 1.5 wt% PDMS	2.36±0.22	1.42±0.35
PTB7:[70]PCBM + 0.3 wt% AXcPDMS	1.36±0.50	0.30±0.14

PTB7:[70]PCBM + 0.03 wt% AXcPDMS	1.39±0.28	1.15±0.36

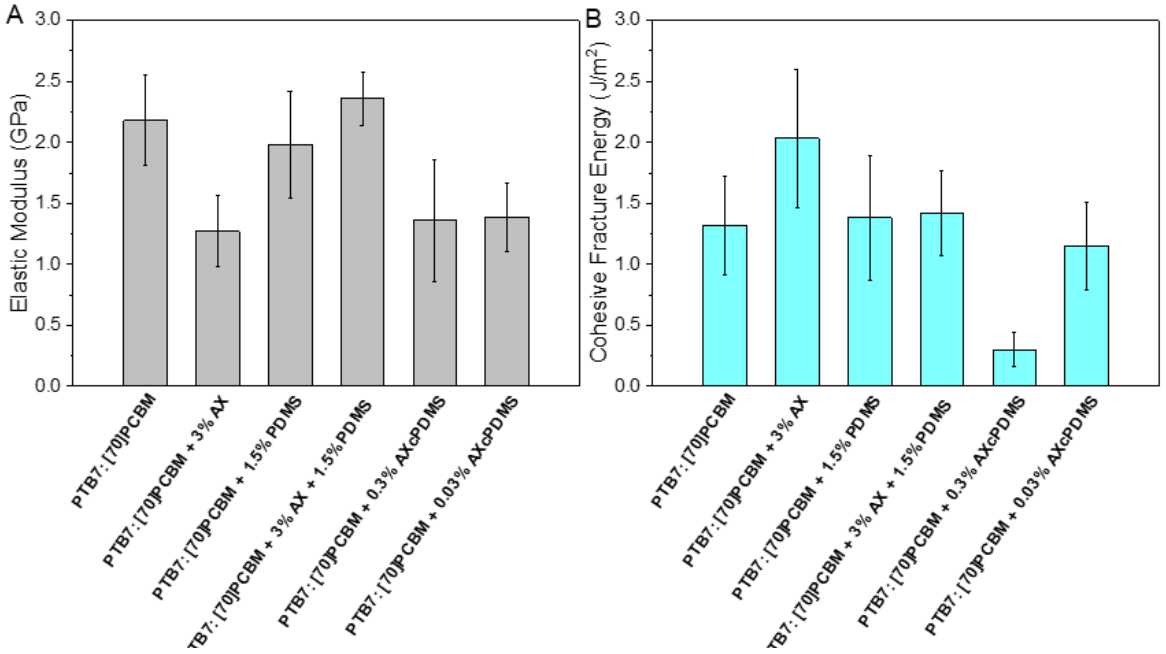

Figure 6 Comparison of a) elastic modulus, Ef, and b) cohesive fracture energies, Gc, of the different PTB7:[70]PCBM bulk heterojunctions with all the additive combinations. Standard deviation is represented with the error bars. In case of the elastic modulus it is derived for each of the active layers from nine measurements taken at three different film thicknesses. For the Cohesive fracture energy, it is calculated on a minimum of three samples.

However, when the covalently bonded combination of AX and PDMS (both 0.3 wt% and 0.03 wt% of AXcPDMS) is added to the active layer, the elastic modulus was significantly reduced to 1.36 ± 0.50 GPa, pointing to enhanced miscibility of the PDMS with the active layer due to the presence of AX grafted to its chains, which has much stronger interactions with both [70]PCBM and PTB7.

While the material stiffness is defined by the elastic modulus, the resistance to fracture is represented by the cohesive fracture energy (G_c). G_c is an important metric for thermomechanical reliability and is indicative of the propensity of a material to handle processing (e.g., roll-to-roll printing) and deployment in the field (83). Figure 6B summarizes the G_c values for active layers with each of the utilized additives, where a higher G_c value points to a system with a higher mechanical integrity (i.e., which requires a higher energy to fracture it) (84). In all the measurements performed with AX and PDMS, the fracture was proven to be cohesive using X-ray photoelectron spectroscopy (XPS) analysis, as reported in Supplementary 6. From Table 3 it is evident that the different additives introduced in the blends affect the cohesive fracture energy of the film differently, with the highest value of 2.03 ± 0.57 J/m^2 recorded for the PTB7:[70]PCBM + 3 wt% AX. The resultant fracture for the PTB7:[70]PCBM + 3 wt% AX films was roughly in the middle of the film showing a pure cohesive rupture. The G_c of films incorporating 3 wt% AX combined with PDMS (1.42 ± 0.35 J/m^2) were slightly lower than of those containing only AX. However, this decrease was not substantial, and the measured fracture energies were comparable to the control PTB7:[70]PCBM, as well as PTB7:[70]PCBM + 1.5 wt% PDMS (1.38 ± 0.52) J/m^2. The similar fracture energies of the films incorporating PDMS (both with and without AX) indicated that the addition of PDMS and AX does not negatively affect the intrinsic adhesion. Furthermore, when AX alone was mixed in the donor/acceptor blend, the film resilience increased, possibly due to hydrogen bonding between the AX and the PTB7. Cheng et al. (85) reported on the improved efficiencies and stability of different polymer: fullerene blends after the H-bonding additive 4,4'-Biphenol (BPO) was introduced in the systems. The observed H-bonding created a lock mechanism in the blend freezing the donor aggregate state and reducing the strong [70]PCBM aggregation that toughens the film. When PDMS is added, it disrupts the bonding between the additive and the donor driving the film back towards the control values. When considering the AXcPDMS additive, the cohesive energy value drops by 84 % and 78 % as compared to the reference sample, with 3 wt% and 0.3 wt% of AXcPDMS in PTB7:[70]PCBM, respectively. However, the mechanical response of the films with the lowest additive concentration of 0.03 wt% AXcPDMS, having a G_c of 1.15 ± 0.36 J/m^2, is comparable to that of the control samples (Table 3). The fracture of the films incorporating AXcPDMS is still cohesive but occurs for higher concentrations closer to the film/glass interface, indicating a higher concentration of the additive at that interface. The overall XPS analysis does therefore suggest that it is the PDMS that drives the fracture propagation in the organic film. This observation is further supported by the fracture occurring roughly in the middle of the films for the relatively low concentration of 0.03 wt% AXcPDMS.

Experimental

Materials[1]

The study was carried out on PTB7:[70]PCBM organic solar cells, where the polymer Poly[[4,8-bis[(2-ethylhexyl) oxy] benzo[1,2-b:4,5-b'] dithiophene-2,6-diyl] [3-fluoro-2-[(2-ethylhexyl) carbonyl] thieno[3,4-b] thiophenediyl]], PTB7 was purchased from 1-material, and the fullerene [70]PCBM was purchased from Solenne. For the additives, succinic anhydride terminated polydimethylsiloxane PDMS100 (DMS-Z21 75-100 cSt, M_w = 800 g mol^{-1}) was purchased from Gelest and Astaxanthin was delivered by CarboSynth. 4-Dimethylaminopyridine (DMAP, ≥ 98 %), silicone oil (PDMS 10000 cSt), and dichloromethane (DCM, ≥ 99.8 %) were purchased from Sigma-Aldrich. Dichloromethane was dried over activated molecular sieves. The processing additive 1,8-diiodooctane, was purchased from Alfa Aesar.

Synthesis of AXcPDMS

Firstly, AX (0.1 g, 0.17 × 10^{-3} mol) and PDMS100 (0.12 g, 0.17 × 10^{-3} mol) were dissolved in 4 mL DCM in a round bottom flask under nitrogen flow at a temperature of 37 °C. Subsequently, the DMAP catalyst (1 × 10^{-2} g, 0.85 × 10^{-4} mol) was added to the reaction mixture. The reaction was stirred overnight, and the product was purified by elution through a silica column using 5 % by volume MeOH/DCM as a mobile phase, in order to remove the catalyst.

Characterization of AXcPDMS

Proton nuclear magnetic resonance (1H NMR) spectra were recorded on a Bruker Advance 300 MHz spectrometer with chloroform-d (CDCl3, 99.8 atom% D) as a solvent. Gel permeation chromatography (GPC) was run with a Viscotec Model 302 instrument, provided with two PLgel mixed-D columns (Polymer Laboratories) assembled in series, and using a UV-vis detector (Knauer) with tetrahydrofuran (1 mL min^{-1}) as the mobile phase. A Polar Star Omega (BMG Labtech) spectrophotometer was used to measure the absorbance spectra (λ = 220-1000 nm).

The additive AXcPDMS was synthesized via a DMAP-catalyzed esterification reaction (Figure 7) between succinic anhydride terminated polydimethylsiloxane (PDMS100) and astaxanthin (AX). A molar ratio PDMS100:AX:DMAP of 1:1:0.5 was used for the reaction. The product was characterized by 1H NMR spectroscopy (Supplementary 8) and UV-vis-detected GPC (Supplementary 9). In the 1H NMR spectrum, the appearance of the signal at resonance δ = 5.4 ppm assigned to the C-H adjacent to the ester linkage between the AX and the PDMS units confirmed successful esterification. GPC traces were analysed by means of a UV-vis detector set at a wavelength λ = 480 nm, corresponding to the characteristic wavelength of maximum absorption of astaxanthin. As expected, the synthesized additive AXcPDMS showed a strong absorbance at a shifted retention volume compared to free astaxanthin (Supplementary 9A). The UV-vis absorbance spectrum of AXcPDMS was also recorded and compared to the free astaxanthin and the observed values of λ_{max} were nearly identical (Supplementary 9B). Based on these results, it can be concluded that the synthetic coupling of PDMS and astaxanthin to obtain the additive AXcPDMS did not affect the structure of conjugated double bonds in the starting reagent astaxanthin, which is fundamental to retain the inherent radical scavenging properties and singlet oxygen quenching capability of the compound.

Thin film and device fabrication

All the samples were produced in a nitrogen filled glovebox with O_2 < 1 ppm and H_20 < 0.1 ppm. For the OPV fabrication, 150 nm thick ITO substrates purchased from Kintec, were cleaned in acetone and isopropyl alcohol (IPA) for 15 min and then treated for 20 min with UV-ozone. A 30 nm layer of ZnO (GenesInk, H-SZ01034) was spin-coated on top of the ITO at 2000 rad/s for 60 s and annealed at 130 °C for 15 min. For the active layers, the reference utilized a weight ratio of 2:3 PTB7:[70]PCBM solution (10 mg of polymer per 1 ml of chlorobenzene with 3 % volume concentration of 1,8-diiodooctane). All the solutions were stirred on hot plate at 85 °C for 2 h prior to spin coating. The active layers were spin-coated uniformly at 1000 rad/s for 120 s to achieve the desired thicknesses. The top layers, MoO_3 (Sigma-Aldrich) and silver (AESpump ApS) were deposited by thermal evaporation at a rate of 0.02 nm/s and 0.05 nm/s to obtain films of 10 nm and 100 nm, respectively.

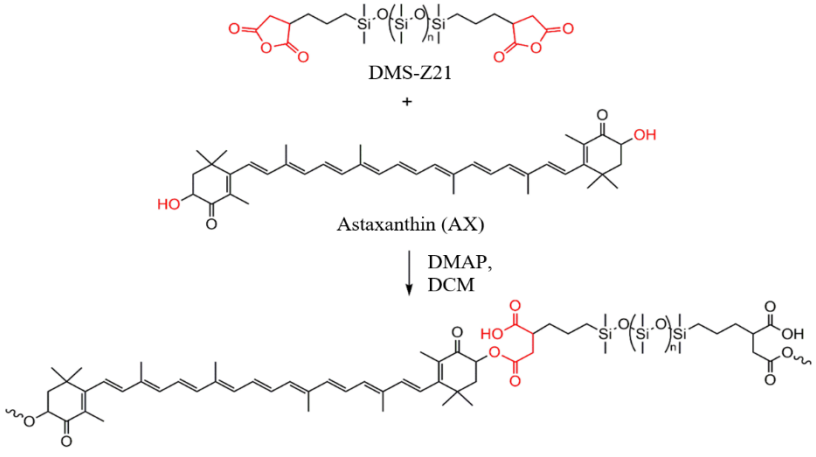

Figure 7 Reaction scheme. Synthesis of AXcPDMS

The intrinsic mechanical properties of the different active layers were defined with the elastic modulus and the cohesive energy measurements of the conjugated polymer films. For both, squared glass slides of 2.5 cm^2 were cleaned in Alconox solution (1 mg/ml), deionized water, acetone, and isopropyl alcohol (IPA) for 10 min each, followed by blow drying. The samples were then plasma treated at 50 W for 3 min to remove organic residuals and activate the surface right before spin-coating the different active layer films.

Device characterization

The J(V) curves were measured by applying a voltage sweep from +1.25 V to −0.25 V using a Keithley 2602a and a class AAA solar simulator (Sun 3000, Abet Technologies Inc., USA) under a lamp calibrated to an intensity of 100 mW/cm^2. The lifetime data were collected in accelerated conditions according to the ISOS-L-2 protocol standards (69), under continuous illumination (AM 1.5G, 100 mW/cm^2) in ambient air, using an InfinityPV ISOSun solar simulator consisting of an Osram metal halide lamp delivering 1 kWm^{-2}. The temperature during the aging process was monitored and kept at 65 °C.

Tensile modulus measurement

The elastic moduli of the different blends were measured using the Buckling on Elastomer technique, first described by Stafford et al. (86). Polydimethylsiloxane (PDMS) substrates were fabricated accordingly to the manufacturer's suggestions in a ratio of 10:1 base:cross-linker and cured for 30 min at 80° C. The PDMS was cut in slabs of 1 cm × 8 cm × 0.3 cm and stretched up to 4 % using a controlled stage. The pre-stretched specimen was then clipped to a microscope glass slide and then the active layer was transferred to this pre-strained substrate. The spin-coated film on glass was gently pressed onto the PDMS substrate and submerged in a beaker containing deionized water, which allowed water to diffuse to the glass/polymer interface achieving the complete transfer of the film to the PDMS. The time in water varied in relation to the active layer composition, ranging from 10 s to 1 min. After transfer, the substrate was gently blow-dried with N_2 and subsequently dried in a desiccator under active vacuum for 20 min. At this point, the strain on the PDMS was released, forming buckles that were finally analysed via an optical microscope. The buckles measurement was performed for different film thicknesses (Supplementary 7) to have a better modulus estimation.

Cohesive fracture energy measurement

The cohesive fracture energy (G_c) of the bulk heterojunction layers was measured by the Double Cantilever Beam (DCB) method, reported elsewhere (84,87–90). Beams were prepared by spin coating the semiconducting layers onto 2.5 mm × 3.75 mm glass slides. On top of these films, a 200 nm Al layer was deposited via e-beam evaporation (1 Å/s). This stack was then adhered to another glass beam using epoxy glue (Loctite EA E20-NS), which was cured for 24 h in air at ambient temperature ~ 25 °C and 20 % R.H. The fracture testing of the DCB was performed under displacement control in a thin-film cohesion testing system (DTS Company, Menlo Park,CA), which measured load (P) versus displacement (Δ). Tension was applied to the specimen at an initial rate of 1 μm/s (which was increased proportionally to the crack length in order to keep the displacement at the crack tip constant) that allowed a pre-initiated crack to propagate. The G_c is then calculated from the following equation:

$$G_c = \frac{12P_c^2a^2}{b^2E'h^3}\left(1 + 0.64\frac{h}{a}\right)^2$$

Where P_c is the critical load at which crack growth occurs, E' is the plane strain elastic modulus, and b and h are the width and half-thickness of the substrates. The crack length, a, can be estimated from the compliance using the following equation:

$$a = \left(\frac{d\Delta}{dP} \times \frac{bE'h^3}{8}\right)^{1/3} - 0.64h$$

The two delaminated sides of the samples were then analysed via X-ray photoelectron spectroscopy (XPS) (Kratos 165 Ultra Photoelectron Spectrometer, scanned 0−1000 eV using monochromatic Al Kα x-ray radiation at 1487 eV) to confirm the cohesive fracture.

Transient PL

The transient photoluminescence signal was recorded using a streak scope coupled to a laser scanning microscope providing time-encoded spectral photoluminescence data. The 395 nm excitation pulses were generated using a sub-100 fs, 75 MHz Ti: Sapphire laser (Spectra Physics, Tsunami) coupled to a frequency converter (APE, HarmoniXX). The repetition rate was reduced by a factor of 20 using a pulse picker (APE, Pulse Select). More information can be found in reference (91).

Singlet oxygen phosphorescence

The equipment and procedures used to record singlet oxygen emission have been described before (44,47). Briefly, the samples were excited at 420 nm using the frequency-doubled output of an amplified Ti: Sapphire laser system (Spectra Physics, Tsunami and Spitfire) operating at 1 kHz repetition rate. The 1275 nm emission from singlet oxygen was isolated with optical filters and recorded using a near-IR sensitive photomultiplier tube (Hamamatsu, R5509-42).

Conclusions

In this work, we investigate the effect of including additives into the active layers of OPV films to concurrently improve both the mechanical properties and photooxidative stability of the device. We demonstrate that while the introduction of the carotenoid astaxanthin, AX, quenches singlet oxygen and its precursor in PTB7:PCBM solar cells, the effect from this molecule on device stability is still limited, showing an enhancement in the accumulated power generation (APG) of 10 %. However, this enhancement is coupled with a drop in the initial device performance. Upon addition of the plasticizer

polydimethylsiloxane (PDMS), the photochemical stability of the devices improves, possibly due to an improved morphology in the active layer blends, as PDMS does not exhibit antioxidant properties. Notably, when adding a newly synthesized additive, AXcPDMS, consisting of AX covalently bonded to PDMS, the photochemical device stability improves further demonstrating an enhancement in APG by 140 %. For this additive, the initial performance remains the same as of the reference cells. Finally, the impact of the additives on the mechanical properties demonstrates an improved elastic modulus and cohesive fracture energy, which is relevant for the mechanical stability of flexible organic solar cell devices. The new AXcPDMS additive provides a lower elastic modulus and keeps the cohesive energy constant leading to a more compliant film, while at the same time enabling a synergistic enhancement of photooxidative stability. As long-lived triplet excited states are also found in novel non-fullerene based systems (92,93), the reported additives hold a great potential for these systems. This study opens up for new strategies of designing additives for future highly efficient and stabile roll-to-roll scale development of flexible organic solar cell devices.

Author Contributions

M.P. wrote the first draft, and all authors contributed with feedback; V.T., M.M., M.P., P.R.O., A.P. and A.L.S. designed the experiments; M.P. and fabricated solar cells; M.P., S.E., V.T. and M.M. carried out and analyzed the lifetime measurements; M.B. and P.R.O. carried out and analyzed singlet oxygen phosphorescence measurements; J.S.L. carried out and analyzed transient photoluminescence spectroscopy measurements; E.O., A.L.S. and M.A.B. synthesized and characterized the new additive molecule; M.P., S.D. and A.P. carried out and analyzed mechanical testing.

Conflicts of interest

There are no conflicts to declare.

Acknowledgements

J.S.L. work was supported by a research grant for Project Impulse-OPV (Grant No. 17677) from VILLUM FONDEN. V.T. acknowledges support from L'Oréal-UNESCO for Women in Science. A.L.S., E.O., H.-G.R., M.B., M.M., M.P., P.R.O., V.T., and acknowledge VILLUM FONDEN for Project CompliantPV (Grant No. 13365). S.E. acknowledges support from the U.S. Department of Commerce, National Institute of Standards and Technology under the financial assistance award 70NANB17H305. All XPS measurements were collected in the Laboratory for Electron Spectroscopy and Surface Analysis in the Department of Chemistry and Biochemistry at the University of Arizona.

Notes and references

[1] Certain commercial equipment, instruments, or materials are identified in this paper to specify the experimental procedure adequately. Such identification is not intended to imply recommendation or endorsement by the National Institute of Standards and Technology, nor is it intended to imply that the materials or equipment identified are necessarily the best available for the purpose.

1. Liu Q, Jiang Y, Jin K, Qin J, Xu J, Li W, et al. 18% Efficiency organic solar cells. Sci Bull. 2020;65(4):272–5.
2. Meng L, Zhang Y, Wan X, Li C, Zhang X, Wang Y, et al. Organic and solution-processed tandem solar cells with 17.3% efficiency. Science (80-). 2018;
3. Brabec CJ, Distler A, Du X, Egelhaaf H, Hauch J, Heumueller T, et al. Material Strategies to Accelerate OPV Technology Toward a GW Technology. Adv Energy Mater. 2020;10(43):2001864.
4. Riede M, Spoltore D, Leo K. Organic Solar Cells—The Path to Commercial Success. Adv Energy Mater. 2021;11(1):2002653.
5. Krebs FC, Espinosa N, Hösel M, Søndergaard RR, Jørgensen M. 25th anniversary article: Rise to power - OPV-based solar parks. Vol. 26, Advanced Materials. John Wiley & Sons, Ltd; 2014. p. 29–39.
6. Zheng Z, Hu Q, Zhang S, Zhang D, Wang J, Xie S, et al. A highly efficient non-fullerene organic solar cell with a fill factor over 0.80 enabled by a fine-tuned hole-transporting layer. Adv Mater. 2018;30:1801801.
7. Yuan J, Zhang Y, Zhou L, Zhang G, Yip HL, Lau TK, et al. Single-Junction Organic Solar Cell with over 15% Efficiency Using Fused-Ring Acceptor with Electron-Deficient Core. Joule. 2019;3(4):1140–51.
8. Doumon NY, Dryzhov M V., Houard F V., Le Corre VM, Rahimi Chatri A, Christodoulis P, et al. Photostability of Fullerene and Non-Fullerene Polymer Solar Cells: The Role of the Acceptor. ACS Appl Mater Interfaces. 2019;11:8310–8.
9. Zhao W, Qian D, Zhang S, Li S, Inganäs O, Gao F, et al. Fullerene-Free Polymer Solar Cells with over 11% Efficiency and Excellent Thermal Stability. Adv Mater. 2016;28(23):4734–9.
10. Savagatrup S, Printz AD, O'Connor TF, Zaretski A V., Rodriquez D, Sawyer EJ, et al. Mechanical degradation and stability of organic solar cells: molecular and microstructural determinants. Energy Environ Sci. 2015;8(1):55–80.
11. Inasaridze LN, Shames AI, Martynov I V., Li B, Mumyatov A V., Susarova DK, et al. Light-induced generation of free radicals by fullerene derivatives: an important degradation pathway in organic photovoltaics? J Mater Chem A. 2017;5(17):8044–50.
12. Greenbank W, Djeddaoui N, Destouesse E, Lamminaho J, Prete M, Boukezzi L, et al. Degradation Behaviour of Scalable Non-Fullerene Organic Solar Cells Assessed by Outdoor and Indoor ISOS Stability Protocols. Energy Technol. 2020;8(12):2194–4288.
13. Ciammaruchi L, Oliveira R, Charas A, Tulus, Von Hauff E, Polino G, et al. Stability of organic solar cells with PCDTBT donor polymer: An interlaboratory study. J Mater Res.

2018;33(13):1909–24.
14. Engmann S, Singh CR, Turkovic V, Hoppe H, Gobsch G. Direct Correlation of the Organic Solar Cell Device Performance to the In-Depth Distribution of Highly Ordered Polymer Domains in Polymer / Fullerene Films. Adv Energy Mater. 2013;1463–72.
15. Fraga I, Topham PD, Bussie P. Unravelling the Photodegradation Mechanisms of a Low Bandgap Polymer by Combining Experimental and Modeling Approaches. J Phys Chem C. 2015;119:2166–76.
16. Lipomi DJ, Chong H, Vosgueritchian M, Mei J, Bao Z. Toward mechanically robust and intrinsically stretchable organic solar cells: Evolution of photovoltaic properties with tensile strain. Sol Energy Mater Sol Cells. 2012;107:355–65.
17. Ye L, Collins BA, Jiao X, Zhao J, Yan H, Ade H. Miscibility–Function Relations in Organic Solar Cells: Significance of Optimal Miscibility in Relation to Percolation. Adv Energy Mater. 2018;8(28):1703058.
18. Xiao J, Ren M, Zhang G, Wang J, Zhang D, Liu L, et al. An Operando Study on the Photostability of Nonfullerene Organic Solar Cells. Sol RRL. 2019;3(7):1900077.
19. Li N, Perea JD, Kassar T, Richter M, Heumueller T, Matt GJ, et al. Abnormal strong burn-in degradation of highly efficient polymer solar cells caused by spinodal donor-acceptor demixing. Nat Commun. 2017;8(1):1–9.
20. Xie Y, Hu X, Yin J, Zhang L, Meng X, Xu G, et al. Butanedithiol Solvent Additive Extracting Fullerenes from Donor Phase To Improve Performance and Photostability in Polymer Solar Cells. ACS Appl Mater Interfaces. 2017;9(11):9918–25.
21. Doumon NY, Wang G, Chiechi RC, Koster LJA, Jan L, Koster A. Relating polymer chemical structure to the stability of polymer:fullerene solar cells. J Mater Chem C. 2017;5:6611–9.
22. Baran D, Ashraf RS, Hanifi DA, Abdelsamie M, Gasparini N, Röhr JA, et al. Reducing the efficiency-stability-cost gap of organic photovoltaics with highly efficient and stable small molecule acceptor ternary solar cells. Nat Mater. 2017;16:363–9.
23. Zhao Q, Xiao Z, Qu J, Liu L, Richter H, Chen W, et al. Elevated Stability and Efficiency of Solar Cells via Ordered Alloy Co-Acceptors. ACS Energy Lett. 2019;4:1106–14.
24. Yu L, Qian D, Marina S, Nugroho FAA, Sharma A, Hultmark S, et al. Diffusion-Limited Crystallization: A Rationale for the Thermal Stability of Non-Fullerene Solar Cells. ACS Appl Mater Interfaces. 2019;
25. Ghasemi M, Hu H, Peng Z, Rech JJ, Angunawela I, Carpenter JH, et al. Delineation of Thermodynamic and Kinetic Factors that Control Stability in Non-fullerene Organic Solar Cells. Joule. 2019;3(5):1328–48.
26. de Zerio AD, Müller C. Glass Forming Acceptor Alloys for Highly Efficient and Thermally Stable Ternary Organic Solar Cells. Adv Energy Mater. 2018;8(28):1702741.
27. Ahmad J, Bazaka K, Anderson LJ, White RD, Jacob M V. Materials and methods for encapsulation of OPV : A review. Renew Sustain Energy Rev. 2013;27:104–17.
28. Giannouli M, Drakonakis VM, Savva A, Eleftheriou P. Methods for Improving the Lifetime Performance of Organic Photovoltaics with Low-Costing Encapsulation. ChemPhysChem. 2015;1134–54.
29. Destouesse E, Top M, Lamminaho J, Rubahn H, Fahlteich J, Madsen M. Slot-die processing and encapsulation of non-fullerene based ITO-free organic solar cells and modules Slot-die processing and encapsulation of non-fullerene based ITO-free organic solar cells and modules. Flex Print Electron. 2019;4(4):45004.
30. Yu D, Yang Y, Chen Z, Tao Y, Liu Y. Recent progress on thin-fi lm encapsulation technologies for organic electronic devices. Opt Commun. 2016;362:43–9.
31. Planes E, Juillard S, Matheron M, Charvin N, Cros S, Qian D, et al. Encapsulation Effect on Performance and Stability of Organic Solar Cells. Adv Mater Interfaces. 2020;7(15):2000293.
32. Uddin A, Upama MB, Yi H, Duan L. Encapsulation of organic and perovskite solar cells: A review. Coatings. 2019.
33. Vasilopoulou M, Yusoff ARBM, Kuganathan N, Bao X, Verykios A, Polydorou E, et al. A carbon-doped tantalum dioxyfluoride as a superior electron transport material for high performance organic optoelectronics. Nano Energy. 2020;70.
34. Xu X, Xiao J, Zhang G, Wei L, Jiao X, Yip HL, et al. Interface-enhanced organic solar cells with extrapolated T80 lifetimes of over 20 years. Sci Bull. 2020;65(3):208–16.
35. Jiang Y, Sun L, Jiang F, Xie C, Hu L, Dong X, et al. Photocatalytic effect of ZnO on the stability of nonfullerene acceptors and its mitigation by SnO 2 for nonfullerene organic solar cells. 1438 | Mater Horiz. 2019;6:1438.
36. Ahmadpour M, Fernandes Cauduro AL, Méthivier C, Kunert B, Labanti C, Resel R, et al. Crystalline molybdenum oxide layers as efficient and stable hole contacts in organic photovoltaic devices. ACS Appl Energy Mater. 2019;2:420–7.
37. Zheng Z, He E, Lu Y, Yin Y, Pang X, Guo F, et al. Benzo[1,2-b :4,5- b ']difuran Polymer-Based Non-Fullerene Organic Solar Cells: The Roles of Non-Fullerene Acceptors and Molybdenum Oxide on Their Ambient Stabilities and Processabilities. ACS Appl Mater Interfaces. 2021;13(13):15448–58.
38. Mushfika BU, Wright M, Mahmud A, Elumalai NK, Mahboubi A, Wang D, et al. Photo-degradation of high e ffi ciency fullerene- free polymer solar cells. Nanoscale. 2017;9:18788–97.
39. Zhang L, Lin B, Hu B, Xu X, Ma W. Blade-Cast Nonfullerene Organic Solar Cells in Air with Excellent Morphology , Efficiency , and Stability. 2018;1800343:1–8.
40. Speller EM, Clarke AJ, Aristidou N, Wyatt MF, Francàs L, Fish G, et al. Toward improved environmental stability of polymer: Fullerene and polymer:Nonfullerene organic solar cells: A common energetic origin of light- A nd oxygen-induced degradation. ACS Energy Lett. 2019;4(4):846–52.
41. Wang C, Shaofei N, Slawomir B, Mats F, Xianjie L. Effects of water vapor and oxygen on non-fullerene small molecule

acceptors. J Mater Chem C. 2019;7:879–86.
42. Turkovic V, Engmann S, Tsierkezos N, Hoppe H, Madsen M, Rubahn HG, et al. Long-term stabilization of organic solar cells using hydroperoxide decomposers as additives. Appl Phys A Mater Sci Process. 2016;112:255.
43. Turkovic V, Engmann S, Tsierkezos N, Hoppe H, Ritter U, Gobsch G. Long-term stabilization of organic solar cells using hindered phenols as additives. ACS Appl Mater Interfaces. 2014;6(21):18525–18537.
44. Bregnhøj M, Prete M, Turkovic V, Petersen AU, Nielsen MB, Madsen M, et al. Oxygen-dependent photophysics and photochemistry of prototypical compounds for organic photovoltaics: inhibiting degradation initiated by singlet oxygen at a molecular level. Methods Appl Fluoresc. 2019;8(1):014001.
45. Turkovic V, Engmann S, Tsierkezos N, Hoppe H, Madsen M, Rubahn HG, et al. Long-term stabilization of organic solar cells using UV absorbers. J Phys D Appl Phys. 2016;49(12).
46. Gasparini N, Salvador M, Strohm S, Heumueller T, Levchuk I, Wadsworth A, et al. Burn-in Free Nonfullerene-Based Organic Solar Cells. Adv Energy Mater. 2017;7(19):1–7.
47. Turkovic V, Prete M, Bregnhøj M, Inasaridze L, Volyniuk D, Obrezkov FA, et al. Biomimetic Approach to Inhibition of Photooxidation in Organic Solar Cells Using Beta-Carotene as an Additive. ACS Appl Mater Interfaces. 2019;11(44):41570–9.
48. Salvador M, Gasparini N, Perea JD, Paleti SH, Distler A, Inasaridze LN, et al. Suppressing photooxidation of conjugated polymers and their blends with fullerenes through nickel chelates. Energy Environ Sci. 2017;10:2005–16.
49. Yan L, Wang Y, Wei J, Ji G, Gu H, Li Z, et al. Simultaneous performance and stability improvement of polymer:fullerene solar cells by doping with piperazine. J Mater Chem A. 2019;7(12):7099–108.
50. Guo JJ, Wu Y, Sun R, Wang W, Guo JJ, Wu Q, et al. Suppressing photo-oxidation of non-fullerene acceptors and their blends in organic solar cells by exploring material design and employing friendly stabilizers. J Mater Chem A. 2019;7(43):25088–101.
51. Li Z, Shan J, Yan L, Gu H, Lin Y, Tan H, et al. The Role of Hydrogen-Bond Between Piperazine and Fullerene Molecules in Stabilizing Polymer:Fullerene Solar Cell Performance. ACS Appl Mater Interfaces. 2020;12(13):15472–81.
52. Li Z, Yan L, Shan J, Gu H, Lin Y, Wang Y, et al. Organic Amines as Targeting Stabilizer at the Polymer/Fullerene Interface for Polymer:PC61BM Solar Cells. Energy Technol. 2020;8(12).
53. Yan L, Yi J, Chen Q, Dou J, Yang Y, Liu X, et al. External load-dependent degradation of P3HT:PC61BM solar cells: Behavior, mechanism, and method of suppression. J Mater Chem A. 2017;5(20):10010–20.
54. Zhang C, Heumueller T, Leon S, Gruber W, Burlafinger K, Tang X, et al. A top-down strategy identifying molecular phase stabilizers to overcome microstructure instabilities in organic solar cells. Energy Environ Sci. 2019;12(3):1078–87.
55. Qin M, Cheng P, Mai J, Lau T-KK, Zhang Q, Wang J, et al. Enhancing Efficiency and Stability of Organic Solar Cells by UV Absorbent. Sol RRL. 2017;1(12):1700148.
56. Savagatrup S, Makaram AS, Burke DJ, Lipomi DJ. Mechanical properties of conjugated polymers and polymer-fullerene composites as a function of molecular structure. Adv Funct Mater. 2014;24(8):1169–81.
57. Kim T, Kim JH, Kang TE, Lee C, Kang H, Shin M, et al. Flexible, highly efficient all-polymer solar cells. Nat Commun. 2015;6(May):1–7.
58. Savagatrup S, Printz AD, Rodriquez D, Lipomi DJ. Best of both worlds: Conjugated polymers exhibiting good photovoltaic behavior and high tensile elasticity. Macromolecules. 2014;47(6):1981–92.
59. Gregori A, Tournebize A, Schumann S, Peisert H, Hiorns RC, Chassé T, et al. The role of donor polymer and PEDOT:PSS formulation on adhesion processes in inverted organic solar cells. Sol Energy Mater Sol Cells. 2018;174(April 2017):25–33.
60. Printz AD, Savagatrup S, Burke DJ, Purdy TN, Lipomi DJ. Increased elasticity of a low-bandgap conjugated copolymer by random segmentation for mechanically robust solar cells. RSC Adv. 2014;4(26):13635–43.
61. Sommerville PJW, Li Y, Dong BX, Zhang Y, Onorato JW, Tatum WK, et al. Elucidating the Influence of Side-Chain Circular Distribution on the Crack Onset Strain and Hole Mobility of Near-Amorphous Indacenodithiophene Copolymers. Macromolecules. 2020;53(17):7511–8.
62. Awartani O, Lemanski BI, Ro HW, Richter LJ, DeLongchamp DM, O'Connor BT. Correlating Stiffness, Ductility, and Morphology of Polymer:Fullerene Films for Solar Cell Applications. Adv Energy Mater. 2013;3(3):399–406.
63. Dupont SR, Voroshazi E, Nordlund D, Dauskardt RH. Morphology and interdiffusion control to improve adhesion and cohesion properties in inverted polymer solar cells. Sol Energy Mater Sol Cells. 2015;132:443–9.
64. Riera-Galindo S, Leonardi F, Pfattner R, Mas-Torrent M. Organic Semiconductor/Polymer Blend Films for Organic Field-Effect Transistors. Adv Mater Technol. 2019;4(9).
65. Scaccabarozzi AD, Stingelin N. Semiconducting:insulating polymer blends for optoelectronic applications - A review of recent advances. J Mater Chem A. 2014;2:10818–24.
66. Ferenczi TAM, Müller C, Bradley DDC, Smith P, Nelson J, Stingelin N. Organic semiconductor: Insulator polymer ternary blends for photovoltaics. Adv Mater. 2011;23(35):4093–7.
67. Scaccabarozzi AD, Basham JI, Yu L, Westacott P, Zhang W, Amassian A, et al. High-density polyethylene - An inert additive with stabilizing effects on organic field-effect transistors. J Mater Chem C. 2020;8:15406–15.
68. Graham KR, Mei J, Stalder R, Shim JW, Cheun H, Steffy F, et al. Polydimethylsiloxane as a macromolecular additive for enhanced performance of molecular bulk heterojunction organic solar cells. ACS Appl Mater Interfaces. 2011;3(4):1210–5.
69. Reese MO, Gevorgyan SA, Jørgensen M, Bundgaard E,

Kurtz SR, Ginley DS, et al. Consensus stability testing protocols for organic photovoltaic materials and devices. Sol Energy Mater Sol Cells. 2011;

70. Soon YW, Cho H, Low J, Bronstein H, McCulloch I, Durrant JR, et al. Correlating triplet yield, singlet oxygen generation and photochemical stability in polymer/fullerene blend films. Chem Commun. 2013;49(13):1291.
71. Razzell-Hollis J, Wade J, Tsoi WC, Soon Y, Durrant J, Kim JS. Photochemical stability of high efficiency PTB7:PC70BM solar cell blends. J Mater Chem A. 2014;2(47):20189–95.
72. Zhou K, Xin J, Ma W. Hierarchical Morphology Stability under Multiple Stresses in Organic Solar Cells. ACS Energy Lett. 2019;4(2):447–55.
73. Billingham NC, Prentice P, Walker TJ. Some effects of morphology on oxidation and stabilization of polyolefins. In: Degradation and Stab of Polyolefins, IUPAC Microsymp on Macromol, 15th. 1976. p. 287–97.
74. Gao Y, Baca AM, Wang B, Ogilby PR. Activation Barriers for Oxygen Diffusion in Polystyrene and Polycarbonate Glasses: Effects of Low Molecular Weight Additives. Macromolecules. 1994;27(24):7041–8.
75. Bosio GN, Breitenbach T, Parisi J, Reigosa M, Blaikie FH, Pedersen BW, et al. Antioxidant β-carotene does not quench singlet oxygen in mammalian cells. J Am Chem Soc. 2013;135(1):272–9.
76. Ogilby PR, Dillon MP, Gao Y, Iu K-K, Kristiansen M, Taylor VL, et al. Polymer Characterization Using Singlet Oxygen Phosphorescence as a Spectroscopic Probe. In: Structure-Property Relations in Polymers. American Chemical Society (ACS); 1993. p. 573–98.
77. Szarko JM, Rolczynski BS, Lou SJ, Xu T, Strzalka J, Marks TJ, et al. Photovoltaic function and exciton/charge transfer dynamics in a highly efficient semiconducting copolymer. Adv Funct Mater. 2014;24(1):10–26.
78. Kraus H, Heiber MC, Väth S, Kern J, Deibel C, Sperlich A, et al. Analysis of Triplet Exciton Loss Pathways in PTB7:PC 71 BM Bulk Heterojunction Solar Cells. Sci Rep. 2016;6.
79. Chow PCY, Albert-Seifried S, Gélinas S, Friend RH. Nanosecond intersystem crossing times in fullerene acceptors: Implications for organic photovoltaic diodes. Adv Mater. 2014;26(28):4851–4.
80. Rao A, Chow PCY, Gélinas S, Schlenker CW, Li CZ, Yip HL, et al. The role of spin in the kinetic control of recombination in organic photovoltaics. Nature. 2013;500(7463):435–9.
81. Kim JH, Noh J, Choi H, Lee JY, Kim TS. Mechanical Properties of Polymer-Fullerene Bulk Heterojunction Films: Role of Nanomorphology of Composite Films. Chem Mater. 2017;29(9):3954–61.
82. O'Connor TF, Zaretski A V., Savagatrup S, Printz AD, Wilkes CD, Diaz MI, et al. Wearable organic solar cells with high cyclic bending stability: Materials selection criteria. Sol Energy Mater Sol Cells. 2016;144:438–44.
83. Balar N, O'Connor BT. Correlating Crack Onset Strain and Cohesive Fracture Energy in Polymer Semiconductor Films. Macromolecules. 2017;50(21):8611–8.
84. Brand V, Bruner C, Dauskardt RH. Cohesion and device reliability in organic bulk heterojunction photovoltaic cells. Sol Energy Mater Sol Cells. 2012;99:182–9.
85. Cheng P, Yan C, Lau TK, Mai J, Lu X, Zhan X. Molecular Lock: A Versatile Key to Enhance Efficiency and Stability of Organic Solar Cells. Adv Mater. 2016;28(28):5822–9.
86. Stafford CM, Harrison C, Beers KL, Karim A, Amis EJ, Vanlandingham MR, et al. A buckling-based metrology for measuring the elastic moduli of polymeric thin films. Nat Mater. 2004;3(8):545–50.
87. Dauskardt RH, Lane M, Ma Q, Krishna N. Adhesion and debonding of multi-layer thin film structures. Eng Fract Mech. 1998;61:141–62.
88. Kim J-H, Lee I, Kim T-S, Rolston N, Watson BL, Dauskardt RH. Understanding mechanical behavior and reliability of organic electronic materials. MRS Bull. 2017;42(02):115–23.
89. Dupont SR, Oliver M, Krebs FC, Dauskardt RH. Interlayer adhesion in roll-to-roll processed flexible inverted polymer solar cells. Sol Energy Mater Sol Cells. 2012;97:171–5.
90. Greenbank W, Rolston N, Destouesse E, Wantz G, Hirsch L, Dauskardt R, et al. Improved mechanical adhesion and electronic stability of organic solar cells with thermal ageing: the role of diffusion at the hole extraction interface. J Mater Chem A. 2017;5(6):2911–9.
91. Cielecki PP, Adam J, Leißner T, Patil BR, Madsen M, Rubahn HG, et al. Photo-induced degradation mechanisms in 4P-NPD thin films. Org Electron. 2018;
92. Wang R, Xu J, Fu L, Zhang C, Li Q, Yao J, et al. Nonradiative Triplet Loss Suppressed in Organic Photovoltaic Blends with Fluoridated Nonfullerene Acceptors. J Am Chem Soc. 2021;143(111).
93. Chen Z, Chen X, Jia Z, Zhou G, Xu J, Wu Y, et al. Triplet exciton formation for non-radiative voltage loss in high-efficiency nonfullerene organic solar cells. Joule. 2021;